Available online at www.sciencedirect.com

SciVerse ScienceDirect

Journal of the European Ceramic Society 32 (2012) 1205–1211

www.elsevier.com/locate/jeurceramsoc

Reaction sintered zirconium titanate–zirconia bulk materials from $3Y_2O_3$-stabilized zirconia and TiO_2. Phase composition and their potential for thermal shock applications

E. López-López [a], I. Santacruz [b], L. Leon-Reina [c], M.A.G. Aranda [b], R. Moreno [a], C. Baudín [a,*]

[a] *Instituto de Cerámica y Vidrio, CSIC, C/Kelsen 5, 28049 Madrid, Spain*
[b] *Departamento de Química Inorgánica, Cristalografía y Mineralogía, Universidad de Málaga, 29071 Málaga, Spain*
[c] *Servicios Centrales de Investigación, Universidad de Málaga, 29071 Málaga, Spain*

Received 20 September 2011; received in revised form 10 November 2011; accepted 19 November 2011
Available online 23 December 2011

Abstract

This work evaluates the potential of zirconium titanate–zirconia composites for thermal shock. Materials with $Zr_{0.97}Y_{0.03}O_{1.985}$:$TiO_2$ molar ratios 50:50 (Z(Y)T50) and 70:30 (Z(Y)T70) were obtained from Y_2O_3 (3 mol%)-stabilized ZrO_2 and TiO_2 mixtures colloidal processed and reaction sintered at 1773 K with low cooling rate (2–5 K/min). The crystalline phases and their unit cell parameters were determined by Rietveld analysis of high resolution X-ray diffraction patterns. The zirconium titanate phase in these materials is o-$TiZrO_4$, being the major phase in Z(Y)T50 in which c-ZrO_2 is secondary phase. Z(Y)T70 has t-ZrO_2 as main phase, o-$TiZrO_4$ as secondary phase and c-ZrO_2 and m-ZrO_2 as minor phases. The Hasselman thermal shock resistance factors, calculated using the experimental values of the involved properties, Young's modulus, thermal expansion coefficient, and fracture strength, have demonstrated the high potential of zirconia–zirconium titanate composites for thermal shock applications in oxidizing atmospheres.

Keywords: A. Suspensions; B. X-ray methods; C. Mechanical properties; Zirconium titanate; E. Structural applications

1. Introduction

Zirconium titanate ($ZrTiO_4$) is a well known compound in the field of electroceramics, where it has been used as constituent of dielectric resonators and devices for telecommunications.[1–6] Zirconium titanate has crystallographic anisotropy in thermal expansion ($\alpha_{a298-1073\,K} = 6.2 \times 10^{-6}\,K^{-1}$, $\alpha_{b298-1073\,K} = 10.0 \times 10^{-6}\,K^{-1}$, $\alpha_{c298-1073\,K} = 8.0 \times 10^{-6}\,K^{-1}$).[7] Thermal expansion mismatch in single phase zirconium titanate materials and/or zirconium titanate based composites would lead to the development of stresses in the materials during cooling from the sintering temperature. For grain sizes above a critical one, such stresses originate cracking through the microstructure[8,9] as occurs in aluminum titanate.[10–12] Cracked materials usually present low thermal expansion and Young's modulus and, consequently, develop low stresses when subjected to thermal shock.[13,14] Such materials, usually referred as low thermal expansion materials, are suitable for structural applications involving temperature variations. Due to the crystallographic anisotropy in thermal expansion zirconium titanate would, in principle, be suitable for the development of thermal shock resistant materials. In spite of this potential there is very limited information in the literature about its thermomechanical behavior as it has only been used as a minor phase to modify the functional properties of other materials and not as bulk material.

This work is part of a wider study dealing with the thermomechanical behavior of zirconium titanate based materials and the evaluation of their actual potential for thermal shock applications. In a previous work,[15] the fabrication of single phase $ZrTiO_4$ bulk materials by solid state reaction of ZrO_2 and TiO_2 and the crystallographic parameters of $ZrTiO_4$ as a function of the cooling rate were reported. The potential of $ZrTiO_4$ bulk samples for thermal shock applications was discussed on the basis of the thermal expansion coefficient and

* Corresponding author.
E-mail address: cbaudin@icv.csic.es (C. Baudín).

0955-2219/$ – see front matter © 2011 Elsevier Ltd. All rights reserved.
doi:10.1016/j.jeurceramsoc.2011.11.024

the indentation Young's modulus determined for the obtained materials.

The single phase materials with grain sizes in the range of 5–8 μm studied in the previous work did not develop cracks on cooling due to the thermal stresses, thus, it has been found that they are not typical low thermal expansion materials such as aluminum titanate. Their potential for thermal shock, evaluated from the product of the average thermal expansion coefficient and the Young's modulus, was similar to that of other uncracked thermal shock resistant oxides such as mullite. This work deals with the phase and microstructural development and the thermal shock resistance potential of zirconia–zirconium titanate composites. In such materials stresses will develop on cooling due to the thermal expansion mismatch between the zirconia and the zirconium titanate grains. The level and sign of the stresses will be dependent on the particular orientation of the grains.

2. Experimental

Commercial ZrO_2 stabilized with 3 mol% of Y_2O_3 (yttria-tetragonal zirconia polycrystal Y-TZP, TZ3YS, TOSOH, Tokyo, Japan) and anatase-TiO_2 (Merck, 808, Darmstadt, Germany) were used as precursor powders. These powders have average particle diameters of 0.4 and 0.3 μm, respectively, and specific surface areas of 6.7 and 9.0 m^2/g, respectively.

Concentrated suspensions of Y-TZP (Z(Y)) and TiO_2 (T) were prepared separately to 45 vol.% solids (83 wt.% and 76 wt.%, respectively) by adding the powder to the proper amount of deionized water containing polyacrylic-based dispersant (Dolapix CE64, Zschimmer-Schwarz, Lahnstein, Germany) to a total concentration of 0.8 wt.% on a dry solids basis, and further mixing with a high shear mixer (Silverson, L2R, Chesham, United Kingdom). Then, they were ball milled for 24 h using alumina jar and balls. The so-prepared one component suspensions were mixed to relative molar ratios of 70:30 and 50:50 (Z(Y):T) in order to obtain Z(Y)T70 and Z(Y)T50 suspensions, respectively. The resulting mixtures were then ball milled for 1 h to assure uniform mixing. Details of the preparation procedure are given in previous works.[16,17] Green plates of about 70 mm × 70 mm × 10 mm in dimensions were obtained by slip casting in plaster molds and drying in air for 48 h.

The final materials, Z(Y)T70 and Z(Y)T50, were obtained after a reaction sintering process at 1773 K/2 h with a heating rate of 5 K/min and a cooling rate of 5 K/min to 1373 K and then 2 K/min to room temperature. This thermal treatment was selected in a previous work.[16] The specimens for the different characterizations were machined from the sintered plates (≈60 mm × 60 mm × 5 mm). Pieces of ≈10 mm × 5 mm × 5 mm were used for density and thermal expansion determinations. The reported results are the averages of three determinations and errors are the standard deviations.

Sintered density was determined by the Archimedes' method using deionized water. Relative densities of the sintered Z(Y)T70 and Z(Y)T50 bulk materials were calculated using the experimental data and the values calculated from the densities and the mass fractions of the constituent phases. The density values of each phase were obtained from the cell parameters determined by the Rietveld method as described below.

X-ray diffraction patterns for the two bulk specimens, Z(Y)T50 and Z(Y)T70, were recorded on a PANalytical X'Pert PRO MPD diffractometer working in reflection geometry ($\theta/2\theta$) and using the X'Celerator RTMS (Real Time Multiple Strip) detector with an active length of 2.122°. The compact flat specimens were loaded in a multi-purpose sample holder which allows the micrometric controlled alignment of samples with a mass up to 1 kg. The patterns were collected with a long fine focus Cu tube working at 45 kV and 40 mA. The incident beam optic path contained a hybrid monochromator (composed of a W/Si parabolic X-ray graded mirror and a flat Ge (2 2 0) asymmetric monochromator) which yielded a strictly monochromatic, λ = 1.54059 Å parallel X-ray beam, and a fixed 1/8° anti-scatter slit. The diffracted beam optic path contained a fixed 1/8° divergence slit. Both, incident and diffracted beams were equipped with 0.02 rad Soller slits. A typical scan range was from 20.0 to 100.0° 2θ with a step size of 0.0167° 2θ and an overall recording time of approximately 4 h. The patterns were analyzed by the Rietveld method[18] using the GSAS program.[19]

The microstructure of diamond polished (down to 3 μm) samples was characterized by scanning electron microscopy (TM-1000 Tabletop, Hitachi, Tokyo, Japan). Energy dispersive X-ray (EDX) analyses were performed by field emission gun-scanning electron microscopy with energy dispersive X-ray (FE-SEM-EDX, Hitachi S-4700 type I, Tokyo, Japan) microanalysis.

The thermal expansion curves were recorded in a differential dilatometer (402 EP, Netzsch, Selb, Germany) using heating and cooling rates of 2 K/min. The average thermal expansion coefficient between room temperature and 1123 K was calculated from the curves. Instrumented indentation tests were performed using a specially developed electromechanical indentation device (Microtest, Madrid, Spain).[20] The indenter is a diamond Vickers pyramid with angle of 136°. Loading was performed in displacement control at a constant rate (0.05 mm/min) up to 100 N. Then, the load was held for 10 s, and finally, unloading was performed at the same rate. Apparent Young's modulus was calculated using the Oliver and Pharr model.[21,22] Vickers hardness was calculated using Eq. (1), where P is the maximum load and a is the length of the semidiagonal of the residual impression measured by optical microscopy (H-P1, Carl-Zeiss, Oberkochen, Germany) with an accuracy of ±3 μm.

$$\mathrm{Hv} = 0.4636 \cdot \frac{P}{a^2} \tag{1}$$

Additionally, mullite (grain size ≈ 1 μm[23] and theoretical density ≈ 97%[24]) and Y-TZP (grain size < 2 μm and theoretical density > 99%[16]) specimens were tested for apparent Young's modulus and hardness.

Bars of 3 mm × 4 mm × 50 mm cut from the sintered blocks were used to determine fracture strength at room temperature in a universal testing machine (EM1/50/FR, Microtest, Madrid, Spain) with inner and outer spans of 20 and 40 mm, respectively. Load was applied with a constant crosshead speed of 0.5 mm/min.

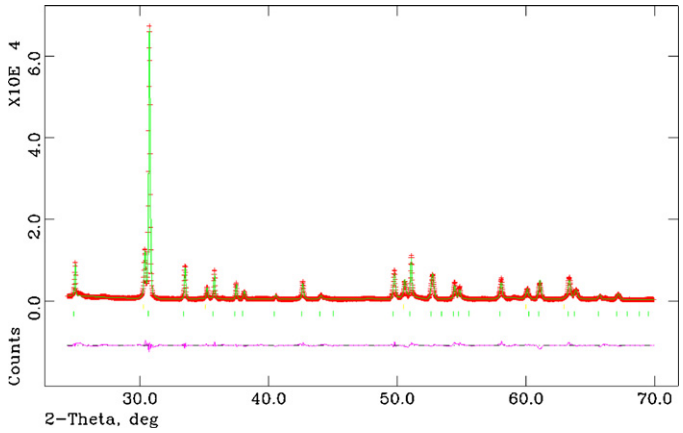

Fig. 1. Observed (crosses), calculated (full line) and difference curve (bottom) X-ray powder diffraction profiles for Z(Y)T50 bulk material. The vertical mark rows give the allowed Bragg peak position for c-ZrO_2 (top) and o-$ZrTiO_4$ (bottom).

3. Results and discussion

Figs. 1 and 2 show the typical Rietveld analyzed high resolution powder X-ray diffraction patterns for Z(Y)T50 and Z(Y)T70, respectively. Initially, the crystalline phases were identified in agreement to the PDF database. Fig. 3 shows a selected region of the powder patterns of the composite specimens studied in this work. For the sake of comparison, the pattern corresponding to a $ZrTiO_4$ single phase material previously studied,[15] is also shown. The appearance of the new phases is clearly highlighted and characteristic peaks of the different phases are labeled with their corresponding Miller indexes.

For Z(Y)T50, only two crystalline phases were identified: orthorhombic $ZrTiO_4$ (PDF 34-0415) and cubic yttrium titanium zirconium oxide (PDF 82-1246). For Z(Y)T70, four crystalline phases were identified: orthorhombic $ZrTiO_4$ (PDF 34-0415), cubic yttrium titanium zirconium oxide (PDF 82-1246), tetragonal yttrium titanium zirconium oxide (PDF 79-1770) and monoclinic zirconium oxide (PDF 37-1484).

According to the 1773 K isothermal sections of the ZrO_2–TiO_2–Y_2O_3 system published by different authors,[25–28] there are some differences about the phases expected for Z(Y)T70 and Z(Y)T50 compositions, as discussed by López-López et al. in a recent review work.[29] These differences show that the ZrO_2–TiO_2–Y_2O_3 system is very sensitive to small compositional and processing changes, thus, the limits between the different phase regions are difficult to establish. According to Colomer et al.[25] and Kobayashi et al.,[26] Z(Y)T70 should be formed by t-ZrO_2ss and $ZrTiO_4$ss, whereas Feighery et al.[27] and Schaedler et al.[28] suggest a phase assemblage formed by t-ZrO_2ss, c-ZrO_2ss and $ZrTiO_4$ss. Results from this work for ZT(Y)70 support the equilibrium relations reported by these latter authors. In the case of Z(Y)T50, all authors agree in the final composition ($ZrTiO_4$ss + c-ZrO_2ss) excepting Feighery et al.[27] who propose a composition made of $ZrTiO_4$ss and $Y_2Ti_2O_7$ss. Results for Z(Y)T50 agree with the majority, in fact, $Y_2Ti_2O_7$ss is not an equilibrium phase at 1773 K in this composition, as discussed in Ref. 30.

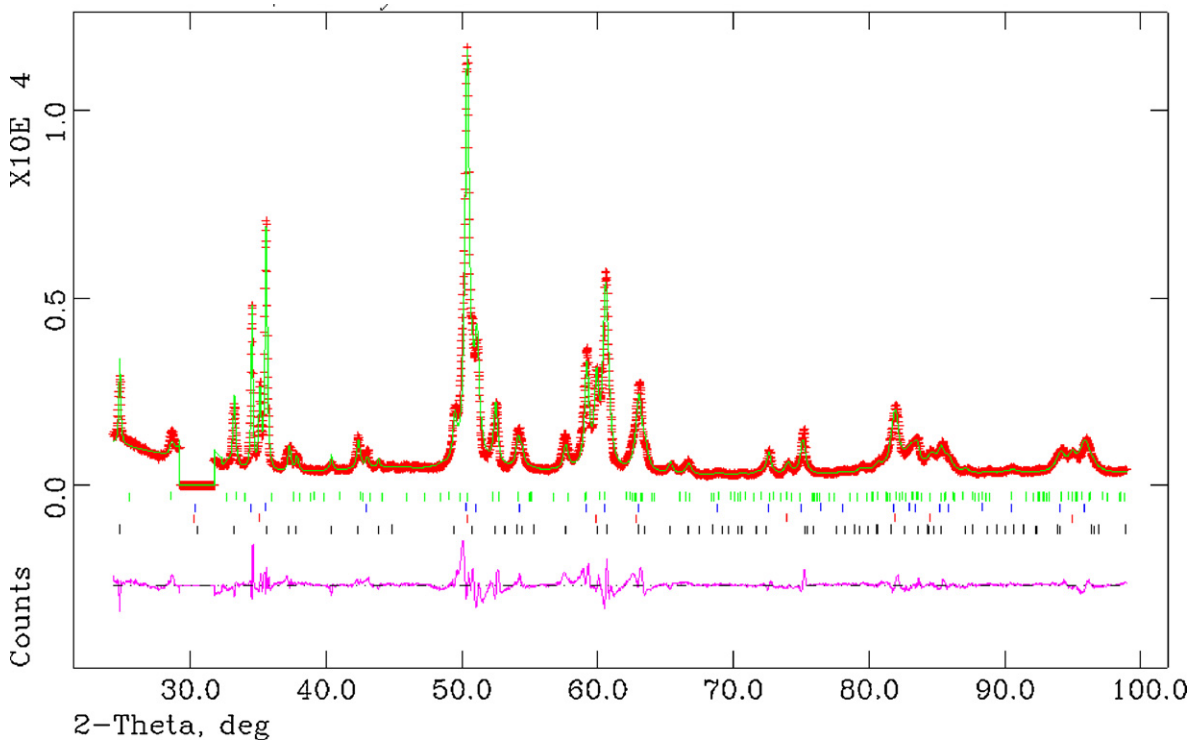

Fig. 2. Observed (crosses), calculated (full line) and difference curve (bottom) X-ray powder diffraction profiles for Z(Y)T70 bulk material. The vertical mark rows give the allowed Bragg peak position for the following phases from top to bottom: m-ZrO_2, t-ZrO_2, c-ZrO_2, and o-$ZrTiO_4$. Due to a problem of the detector electronics in the region 29.2–31.73 (2θ) of the powder pattern of Z(Y)T70, this region was excluded from the refinement.

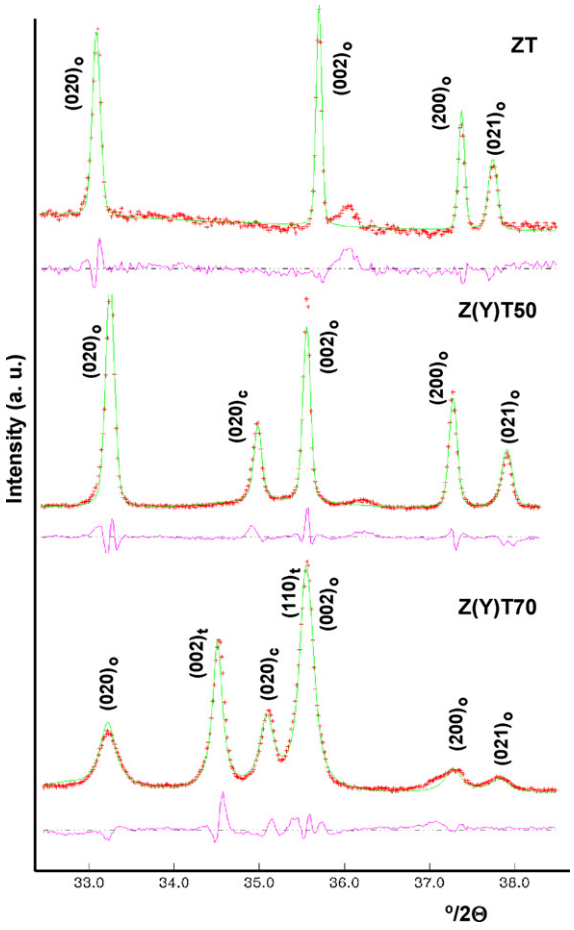

Fig. 3. Selected region of the laboratory X-ray bulk-specimen diffraction patterns for ZT (top),[15] Z(Y)T50 (intermediate) and Z(Y)T70 (bottom). This region is selected to show the phase evolution from single phase o-$ZrTiO_4$ in the top pattern[15] to the phase coexistence of t-ZrO_2, c-ZrO_2, and o-$ZrTiO_4$ in the bottom pattern.

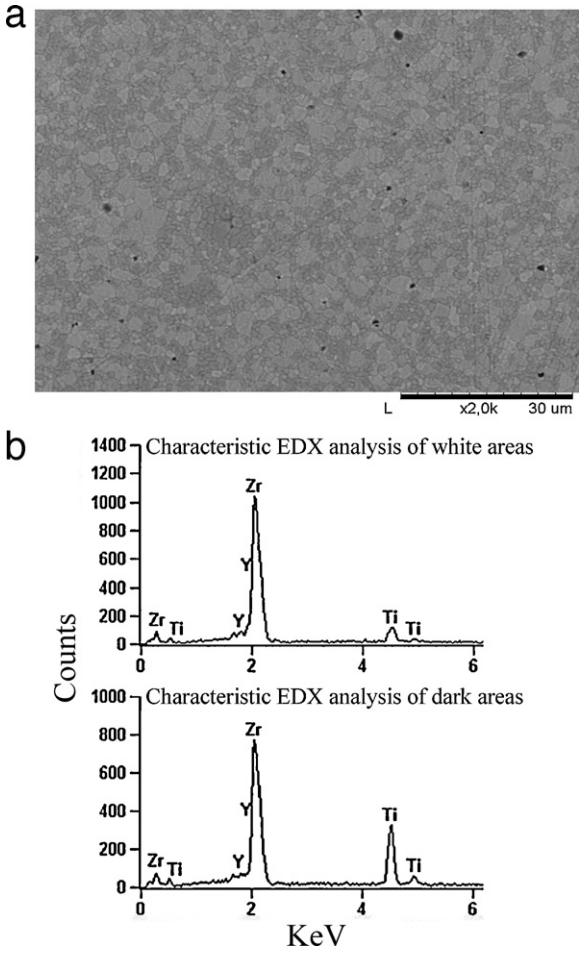

Fig. 4. Microstructure of Z(Y)T70 material. SEM micrograph of a polished and thermally etched (1673 K/1 min) surface (a), together with characteristic EDX analyses (b). Dark areas correspond to $ZrTiO_4$, meanwhile white areas correspond to ZrO_2.

Results from this work demonstrate that the high temperature phases remain in the studied materials with low amounts of Y_2O_3 (<3 mol%) obtained using relatively low cooling rates, such as those characteristic of ceramic processing. In particular, results of the Rietveld analysis of the high resolution powder X-ray diffraction patterns have shown that $ZrTiO_4$ is the only zirconium titanate phase, not being possible $Zr_5Ti_7O_{24}$ as reported in previous works.[16,17,30]

The approximate elemental content of the phases was estimated from the value of unit cell parameters taken into account in the previous structural reports. Hereafter, o-$TiZrO_4$ is used to describe the stoichiometric phase[15]; c-ZrO_2 ICSD-75316 is used to describe a cubic phase with composition close to $Y_{0.18}Ti_{0.22}Zr_{0.60}O_{1.91}$[31]; t-$ZrO_2$ ICSD-66788 is used to describe a tetragonal phase with composition close to $Y_{0.05}Ti_{0.30}Zr_{0.65}O_{1.975}$[32]; and m-$ZrO_2$ ICSD-89426 is used to describe a monoclinic phase with composition close to stoichiometric ZrO_2.[33]

Quantitative results of the study are given in Table 1. In addition to the unit cell parameters, the crystallographic densities and the phase contents are also reported. The quantitative analysis of the final Rietveld fit to the Z(Y)T50 data showed that the main constituent is o-$TiZrO_4$, as expected, and that there is an 11.7 wt.% of c-ZrO_2. The final Rietveld fit to the Z(Y)T70 powder pattern data (Fig. 2) was much more complex than that for Z(Y)T50, with quite broad peaks. The phase assemblage for this material given in Table 1 shows that the main phase is t-ZrO_2.

Fig. 4 shows the microstructure of the Z(Y)T70 sintered material showing the presence of two kinds of grains and the lack of microcracks. Taking into account the phase content in this material and the EDX analyses shown in this figure, it can be concluded that dark grains correspond to $ZrTiO_4$ and white grains to ZrO_2. However, it is not possible to differentiate among the different zirconia phases, t-ZrO_2, c-ZrO_2 and m-ZrO_2.

Fig. 5 shows the microstructure of the Z(Y)T50 sintered material, which was fully characterized in a previous work.[30] The major phase (dark grains) is $ZrTiO_4$, the second phase (white grains) is c-ZrO_2, while there are small (<2 μm) particles located at the $ZrTiO_4$/c-ZrO_2 boundaries which likely correspond to a pyrochlore compound in very minor content. Microcracks of similar size to the zirconium titanate grain diameters are distributed through the whole microstructure.

Table 2 shows absolute and relative density, average thermal expansion coefficient between 298 and 1123 K ($\alpha_{298-1123}$),

Table 1
Crystallographic details (unit cell parameters, density values and phase contents) for Z(Y)T70 and Z(Y)T50 sintered materials determined by the Rietveld method.

Sample	a (Å)	b (Å)	c (Å)	V (Å^3)	ρ (g/cm^3)	Contents (wt.%)
Z(Y)T50[a]						
o-$ZrTiO_4$	4.8087(1)	5.3630(1)	5.0301(1)	129.72(1)	5.20	88.4(8)
c-ZrO_2	5.1120(4)	–	–	133.59(3)	5.56	11.7(2)
Z(Y)T70						
o-$ZrTiO_4$	4.8310(5)	5.4027(5)	5.0497(5)	131.80(3)	5.12	33.8(3)
c-ZrO_2	5.1244(3)	–	–	134.57(3)	5.52	17.2(3)
t-ZrO_2	3.5802(2)	–	5.2102(3)	66.79(1)	5.67	47.8(2)
m-ZrO_2	4.70(1)	5.37(2)	5.37(1)	132.9(3)	6.16	1.1(1)

[a] There is a third minor phase in this material.[30]

Table 2
Absolute (ρ) and relative ($\rho_{relative}$) density, average thermal expansion coefficient between 298 and 1123 K ($\alpha_{298–1123}$), Vickers hardness (Hv), apparent Young's modulus (E_{app}) and fracture strength (σ_f) values for Z(Y)T70, Z(Y)T50, mullite, Y-TZP and YSZ materials.

Material	ρ (g/cm^3)	$\rho_{relative}$ (% T.D.)	$\alpha_{298–1123\,K}$ ($\times10^{-6}$ K^{-1})	Hv (GPa)	E_{app} [a] (GPa)	σ_f (MPa)
Z(Y)T70	5.48 ± 0.02	>99	9.7 ± 0.2	10.2 ± 0.3	125 ± 7	270 ± 28
Z(Y)T50	5.02 ± 0.01	≈96	7.5 ± 0.2	7.5 ± 0.2	64 ± 3	60 ± 3
Mullite	–	≈97[23]	4.1 ± 0.1[23]	11.0 ± 0.4	159 ± 25[15]	228 ± 35[24]
Y-TZP (t-ZrO_2)	6.1 ± 0.1[16]	>99	10.6 ± 0.2[16]	12.8 ± 0.2	188 ± 17	≈1040[34]
YSZ (c-ZrO_2)	–	≈99[35]	10.5[36]	–	≈190[b]	276 ± 49[35]

[a] Calculated from the unload portion of the instrumented indentation load–penetration depth curves.
[b] Estimated data taking into account that dynamic Young's modulus values from Y-TZP and YSZ materials reported in the literature are very similar ≈220 GPa.[39]

Vickers hardness (Hv), apparent Young's modulus (E_{app}) and fracture strength (σ_f) values of Z(Y)T70 and Z(Y)T50 materials. For comparison purposes, the values for a dense and fine grained mullite[15,23] and for two Y_2O_3 stabilized zirconias, t-ZrO_2 (Y-TZP)[16,34] and c-ZrO_2 (YSZ),[35,36] are also reported. Values of $\alpha_{298–1123}$, Hv and E_{app} for dense single phase ZT material evaluated in a previous work[15] were lower than those for t-ZrO_2[16] and c-ZrO_2.[36] Therefore, all properties are lower for Z(Y)T50 than for Z(Y)T70 that contains a higher ZrO_2 amount and does not present microcracks.

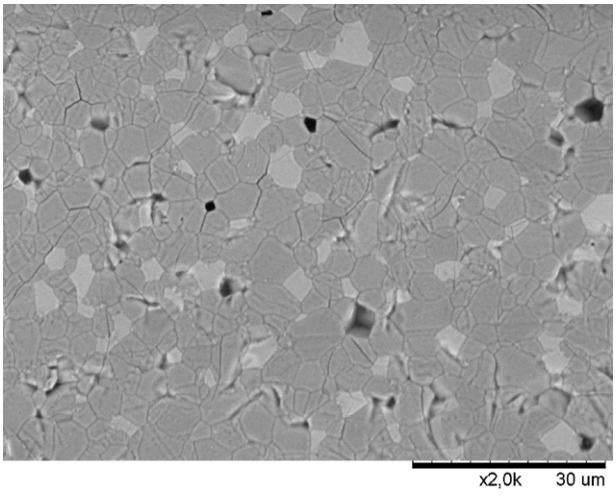

Fig. 5. Microstructure of Z(Y)T50 material. SEM micrograph of a polished and thermally etched surface (1673 K/1 min). Major phase (dark grains) corresponds to $ZrTiO_4$, meanwhile the second phase (white grains) corresponds to c-ZrO_2 solid solution. Microcracks can be observed.

From the average thermal expansion coefficient values in Table 2 it is clear that, as occurred for the monophase ZT studied previously,[15] neither Z(Y)T70 nor Z(Y)T50 can be considered as typical low thermal expansion coefficient materials such as those based on aluminum titanate. The fact that microcrack sizes in Z(Y)T50 are limited to grain sizes results in a thermal expansion coefficient higher than those corresponding to materials with generalized large cracks (e.g. aluminum titanate materials, $\alpha \approx 1.7 \times 10^{-6}$ K^{-1} [37]). However, both materials present relatively lower Young's modulus as compared to other oxides, thus, the product, $E \times \alpha$,[13,14] that determines the thermal stresses developed due to a thermal shock, is lower for Z(Y)T50 and Z(Y)T70 than for cubic and tetragonal zirconia. For Z(Y)T50, $E \times \alpha$ product is even lower than that of mullite, a classical thermal shock resistance oxide (Table 3).

Table 3 reports two classical thermal shock resistance factors of merit established by Hasselman[13,38] that evaluate the resistance of materials to initiation, R, and propagation, R''', of cracks due to thermal shock calculated for the studied materials and other reference oxides. From this data, the critical temperature interval for crack initiation, ΔT_c, evaluated by R, will be the lowest for the microcracked composite, Z(Y)T50, however, damage resistance will be much higher for this material than for the others, as its corresponding R''' is about one order of magnitude higher than those for mullite and c-ZrO_2. Therefore, Z(Y)T50 will have potential in thermal shock applications involving long time under-critical solicitations such as thermal cycling.

The R parameter for composite Z(Y)T70 is higher than that of YSZ and about two thirds of that for mullite, thus, these three materials will have similar resistances to crack initiation. A comparison of expected relative damage resistance based on this parameter might under-evaluate the potential of materials

Table 3
Evaluation of the potential of materials Z(Y)T70 and Z(Y)T50 for thermal shock applications compared to that of uncracked oxides, mullite, Y-TZP and YSZ. Stresses developed, $E \times \alpha$, and parameters of Hasselman[13,38]; calculations have been done considering the properties in Table 2.

Material	$E \times \alpha$ (MPa K^{-1})	$R = \frac{\sigma_f}{E \times \alpha}$ (K)[a]	$R''' = \frac{E}{\sigma_f^2}$ (m^2/N)[a]
Z(Y)T70	1.21 ± 0.09	223 ± 7	$1.7 \pm 0.3 \times 10^{-6}$ [b]
Z(Y)T50	0.48 ± 0.04	125 ± 4	$17.8 \pm 0.9 \times 10^{-6}$
Mullite	0.65 ± 0.12	351 ± 11	$3.1 \pm 0.5 \times 10^{-6}$
Y-TZP (t-ZrO_2)	≈2	≈522	$\approx 0.2 \times 10^{-6}$ [b]
YSZ (c-ZrO_2)	≈2	≈138	$\approx 2.5 \times 10^{-6}$

[a] Poisson's ratio is not considered.
[b] R''' does not take into account the *R*-curve behavior of materials containing t-ZrO_2 (Y-TZP and Z(Y)T70).

containing transformable t-ZrO_2 such as Y-TZP and Z(Y)T70 as they present *R*-curve during fracture. Therefore, the fact that the calculated R''' value is of the same order as that for YSZ, two thirds of that of mullite and one order of magnitude higher than that of Y-TZP, reveals the high potential of such kind of ZT-containing composites for thermal shock applications in oxidizing atmospheres.

4. Conclusions

Large specimens (≈60 mm × 60 mm × 5 mm) of two bulk materials with $Zr_{0.97}Y_{0.03}O_{1.985}$:$TiO_2$ molar ratios of 50:50 (Z(Y)T50) and 70:30 (Z(Y)T70) have been processed using a typical ceramic route involving colloidal green processing and a temperature treatment at 1773 K with low cooling rate (2–5 K/min).

The crystalline phase assemblages and the unit cell parameters of the constituent phases have been determined by Rietveld analysis of high resolution powder X-ray diffraction patterns. It has been demonstrated that o-$TiZrO_4$ is the only zirconium titanate phase in these materials with low amounts of Y_2O_3 (<3 mol%) and obtained using relatively low cooling rates. This is the major phase in Z(Y)T50 in which c-ZrO_2 is the only secondary phase. t-ZrO_2 is the main phase in Z(Y)T70, o-$TiZrO_4$ is the secondary phase and c-ZrO_2 and m-ZrO_2 are minor phases.

The thermal shock resistance factors of merit proposed by Hasselman calculated using the experimental values of the involved properties for the studied materials have demonstrated the high potential of zirconia–zirconium titanate composites for thermal shock applications in oxidizing atmospheres.

Acknowledgments

The work in Madrid has been supported by Spanish Ministry of Science and Innovation under contract MAT2009-14369-C02-01. E. López-López acknowledges to Community of Madrid (Spain) and European Social Fund for economical support by CPI/0552/2007 contract. The work in Málaga has been supported by the research grant FQM-113 from Junta de Andalucía (Spain) and Spanish Ministry of Science and Innovation through a Ramón y Cajal fellowship (RYC-2008-03523).

References

1. Park Y, Kim Y. Influence on cooling rate on the physical properties of tin modified zirconium titanate. *J Mater Sci Lett* 1996;**15**:853–5.
2. Wolfram G, Göbel HE. Existence range, structural and dielectric properties of $Zr_xTi_ySn_zO_4$ ceramics ($X+Y+Z=2$). *Mater Res Bull* 1981;**16**:1455–63.
3. Bianco A, Gusmano G, Freer R, Smith P. Zirconium titanate microwave dielectrics prepared via polymeric precursor route. *J Eur Ceram Soc* 1999;**19**:959–63.
4. Hirano S, Hayashi T, Hattori A. Chemical processing and microwave characteristic of (Zr,Sn)TiO_4 microwave dielectrics. *J Am Ceram Soc* 1991;**74**:1320–4.
5. Christoffersen R, Davies PK, Wei X, Negas T. Effect of Sn substitution on cation ordering in ($Zr_{1-x}Sn_x$)TiO_4 microwave dielectric ceramics. *J Am Ceram Soc* 1994;**77**:441–50.
6. Victor P, Bhattacharyya S, Krupanidhi SB. Dielectric relaxation in laser ablated polycrystalline $ZrTiO_4$ thin films. *J Appl Phys* 2003;**94**:5135–42.
7. Ikawa H, Iwai A, Hiruta K, Shimojima H, Urabe K, Udagawa S. Phase transformation and thermal expansion of zirconium and hafnium titanates and their solid solutions. *J Am Ceram Soc* 1988;**71**:120–7.
8. Kuszyk J, Bradt RC. Influence of grain size on effects of thermal expansion anisotropy in Mg_2TiO_5. *J Am Ceram Soc* 1973;**56**:420–3.
9. Cleveland JJ, Bradt RC. Granin size/microcracking relationships for pseudobrookites oxides. *J Am Ceram Soc* 1978;**61**:478–81.
10. Ohya Y, Nakagawa Z. Grain-boundary microcracking due to thermal expansion anisotropy in aluminium titanate ceramics. *J Am Ceram Soc* 1987;**70**:C-184–6.
11. Parker FJ, Rice RW. Correlation between grain size and thermal expansion for aluminium titanate materials. *J Am Ceram Soc* 1989;**72**:2364–6.
12. Bueno S, Moreno R, Baudin C. Design and processing of Al_2O_3–Al_2TiO_5 layered structures. *J Eur Ceram Soc* 2005;**25**:847–56.
13. Hasselman DPH. Unified theory of thermal shock fracture initiation and crack propagation in brittle ceramics. *J Am Ceram Soc* 1969;**52**:600–4.
14. Uribe R, Baudín C. Influence of a dispersion of aluminium titanate particles of controlled size on the thermal shock resistance of alumina. *J Am Ceram Soc* 2003;**86**:846–50.
15. López-López E, Baudín C, Moreno R, Santacruz I, León-Reina L, Aranda MAG. Structural characterization of bulk $ZrTiO_4$ and its potential for thermal shock applications. *J Eur Ceram Soc* 2012;**32**:299–306.
16. López-López E, Baudín C, Moreno R. Thermal expansion of zirconia–zirconium titanate materials obtained by slip casting of mixtures of Y-TZP-TiO_2. *J Eur Ceram Soc* 2009;**29**:3219–25.
17. López-López E, Baudín C, Moreno R. Synthesis of zirconium titanate-based materials by colloidal filtration and reaction sintering. *Int J Appl Ceram Technol* 2008;**5**:394–400.
18. Rietveld HM. A profile refinement method for nuclear and magnetic structures. *J Appl Cryst* 1969;**2**:65–71.
19. Larson AC, Dreele RBV. Los Alamos National Laboratory. Report No. LA-UR-86-7 48; 2000.
20. Bueno S, Baudín C. Instrumented Vickers microindentation of alumina-based materials. *J Mater Res* 2006;**21**:161–73.

21. Oliver WC, Pharr GM. An improved technique for determining hardness and elastic modulus using load and displacement sensing indentation experiments. *J Mater Res* 1992;**7**:1564–83.
22. Oliver WC, Pharr GM. Measurement of hardness and elastic modulus by instrumented indentation: advances in understanding and refinements to methodology. *J Mater Res* 2004;**19**:3–20.
23. Burgos-Montes O, Moreno R, Baudín C. Effect of mullite additions on the fracture mode of alumina. *J Eur Ceram Soc* 2010;**30**:857–63.
24. Osendi MI, Baudín C. Mechanical properties of mullite materials. *J Eur Ceram Soc* 1996;**16**:217–24.
25. Colomer MT, Durán P, Caballero A, Jurado JR. Microstructure, electrical properties and phase equilibria relationships in the ZrO_2–Y_2O_3–TiO_2 system: the subsolidus isothermal section at 1500 °C. *Mater Sci Eng A* 1997;**229**:114–22.
26. Kobayashi K, Kato K, Terabe K, Yamaguchi S, Iguchi Y. Phase relation of ZrO_2–$YO_{1.5}$–TiO_2 ceramics prepared by sol–gel method. *J Ceram Soc Jpn* 1998;**106**:860–6.
27. Feighery AJ, Irvine JTS, Fagg DP, Kaiser A. Phase relations at 1500 °C in the ternary system ZrO_2–Y_2O_3–TiO_2. *J Solid State Chem* 1999;**143**:273–6.
28. Schaedler TA, Fabrichnaya O, Levi CG. Phase equilibria in the TiO_2–$YO_{1.5}$–ZrO_2 system. *J Eur Ceram Soc* 2008;**28**:2509–20.
29. López-López E, Moreno R, Baudín C. Titanato de circonio: estabilidad termodinámica y expansión térmica. *Bol Soc Esp Ceram V* 2011;**50**:169–76.
30. López-López E, Sanjuán ML, Moreno R, Baudín C. Phase evolution in reaction sintered zirconium titanate based materials. *J Eur Ceram Soc* 2010;**30**:981–91.
31. Yashima M, Sasaki S, Kakihana M, Yamaguchi Y, Arashi H, Yoshimura M. Oxygen-induced structural change of the tetragonal phase around tetragonal-cubic phase boundary in ZrO_2–$YO_{1.5}$ solid solutions. *Acta Crystall B* 1994;**50**:663–72.
32. Bondars B, Heidemename G, Grabis J, Laschke K, Boysen H, Schenider J, et al. Powder diffraction investigations of plasma sprayed zirconia. *J Mater Sci* 1995;**30**:1621–5.
33. McMurdie H, Morris M, Evans E, Paretzkin B, Wong-Ng W, Hubbard C. Standard X-ray diffraction powder patterns from the JCPDS research associateship. *Powder Diffr* 1986;**1**:265–75.
34. Stevens R. Engineering properties of zirconia. In: Scheneider Jr SJ, editor. *Engineered materials handbook*, vol. 4. ASM International; 1991. p. 775–86.
35. Donzel L, Roberts SG. Microstructure and mechanical properties of cubic zirconia (8YSZ)/SiC nanocomposites. *J Eur Ceram Soc* 2000;**20**: 2457–62.
36. Liu ZG, Ouyang JH, Zhou Y. Influence of gadolinia on thermal expansion property of ZrO_2–4.5 mol% Y_2O_3 ceramics. *J Alloys Compd* 2009;**473**:L17–9.
37. Milosevski M, Ondracek O, Milisevska R, Spaseska D, Dimeska A.Thermal expansion and mechanical properties of Al_2TiO_5–SiO_2 system. *Adv Sci Technol* 1995:1875–82.
38. Hasselman DPH. Elastic energy at fracture and surface energy as design criteria for thermal shock. *J Am Ceram Soc* 1963;**46**:535–40.
39. Selçuk A, Atkinson A. Elastic properties of ceramics oxides used in solid oxide fuel cells (SOFC). *J Eur Ceram Soc* 1997;**17**:1523–32.